ACCEPTED MANUSCRIPT

Glassy Carbon MEMS for Novel Origami-Styled 3D Integrated Intracortical and Epicortical Neural Probes

Glassy Carbon MEMS for Novel Origami-Styled 3D Integrated Intracortical and Epicortical Neural Probes

Noah Goshi[a], Elisa Castagnola[a,b], Maria Vomero[c*], Calogero Gueli[c], Claudia Cea[a,b], Elena Zucchini[d], David Bjanes[b,e], Emma Maggiolini[d], Chet Moritz[b,f], Sam Kassegne[a,b], Davide Ricci[d], Luciano Fadiga[d,g]

a. MEMS Research Lab., Department of Mechanical Engineering, College of Engineering, San Diego State University, 5500 Campanile Drive, San Diego, CA 92182-1323, USA

b. Center for Sensorimotor Neural Engineering (CSNE), Box 37, 1414 NE 42nd St., Suite 204, Seattle, WA 98105-6271, USA

c. Laboratory for Biomedical Microsystems, Institute for Microsystem Technology (IMTEK), University of Freiburg, Georges-Köhler-Allee 103, 79110 Freiburg im Breisgau, Germany

d. Center for Translational Neurophysiology of Speech and Communication, Istituto Italiano di Tecnologia, Via Fossato di Mortara 17/19, 44121, Ferrara, Italy

e. University of Washington, Department of Electrical Engineering, Seattle, WA

f. University of Washington, Division of Physical Therapy, Departments of Rehabilitation Medicine and Physiology and Biophysics, Seattle, WA

g. Section of Human Physiology, University of Ferrara, Via Fossato di Mortara 17/19, 44121, Ferrara, Italy

* Previously at MEMS Research Lab., Department of Mechanical Engineering, College of Engineering, San Diego State University, 5500 Campanile Drive, San Diego, CA 92182-1323, USA

e-mail address of each author: nkgoshi@ucdavis.edu ecastagnola@sdsu.edu maria.vomero@imtek.uni-freiburg.de claudia.cea90@gmail.com gerozte@gmail.com elena.zucchini@iit.it davidbjanes@gmail.com emma.maggiolini@iit.it ctmoritz@uw.edu kassegne@mail.sdsu.edu davide.ricci@iit.it luciano.fadiga@iit.it

Correspondence and requests for materials should be addressed to **Elisa Castagnola** e-mail: ecastagnola@sdsu.edu

Full postal address: MEMS Research Lab., EIS Building, Department of Mechanical Engineering, College of Engineering, San Diego State University, 5500 Campanile Drive, San Diego, CA 92182-1323, USA.

Abstract

We report on a novel technology for microfabricating 3D origami-styled Micro Electro-Mechanical Systems (MEMS) structures with glassy carbon (GC) features and a supporting polymer substrate. GC MEMS devices that open to form 3D microstructures are microfabricated from GC patterns that are made through pyrolysis of polymer precursors on high-temperature resisting substrates like silicon or quartz and then transferring the patterned devices to a flexible substrate like polyimide followed by deposition of an insulation layer. The devices on flexible substrate are then folded into 3D form in an origami-fashion.

These 3D MEMS devices have tunable mechanical properties that are achieved by selectively varying the thickness of the polymeric substrate and insulation layers at any desired location. This technology opens new possibilities by enabling microfabrication of a variety of 3D GC MEMS structures suited to applications ranging from biochemical sensing to implantable microelectrode arrays. As a demonstration of the technology, a neural signal recording microelectrode array platform that integrates both surface (cortical) and depth (intracortical) GC microelectrodes onto a single flexible thin-film device is introduced.

When the device is unfurled, a pre-shaped shank of polyimide automatically comes off the substrate and forms the penetrating part of the device in a 3D fashion. With the advantage of being highly reproducible and batch-fabricated, the device introduced here allows for simultaneous recording of electrophysiological signals from both the brain surface (electrocorticography - ECoG) and depth (single neuron). Our device, therefore, has the potential to elucidate the roles of underlying neurons on the different components of μECoG signals. For *in-vivo* validation of the design capabilities, the recording sites are coated with a poly(3,4-ethylenedioxythiophene) - polystyrene sulfonate - carbon nanotube composite, to improve the electrical conductivity of the electrodes and consequently the quality of the recorded signals. Results show that both μECoG and intracortical arrays were able to acquire neural signals with high-sensitivity that increased with depth, thereby verifying the device functionality.

2

Keywords: MEMS, Origami Structures, Microelectrode array (MEA), Thin-film technology, μECoG, intracortical electrode, Glassy Carbon, PEDOT-PSS-CNT coating.

1. Introduction

Carbon, as a technology material, is finding a renewed research and industrial interest. As evidenced by the continued interest in graphene and other forms of carbon such as fullerene, carbon nanotubes (CNT), carbon nanofibers, carbon nano-composites, etc., carbon is poised to become a critical technology material with wide application in a variety of disciplines [**1-3**]. In addition to the traditional areas where the superior electrical and electrochemical properties of carbon have made it a material of choice, recently a renewed focus to this material has been brought by bioengineering research aimed to electrically interfacing it with biological tissues. In turn, these factors have highlighted the need for innovation in robust and versatile micro and nanofabrication technology of carbon-based devices to meet this increasing demand. In response to that, the field of glassy carbon MEMS (GC MEMS), which involves the patterning of a photosensitive polymer precursor on a silicon substrate followed by pyrolysis of the polymer layer to convert it to glassy carbon, has gained traction and increased range of applications [4-6].

Further, the recent introduction of a new pattern transfer technology that allowed GC structures to be supported on polymeric substrates as opposed to only high-temperature resistant silicon and quartz, has enabled GC MEMS technology to enter a new phase [6-8]. This new pattern transfer technology has been demonstrated through the microfabrication of a glassy carbon-based array of microelectrodes on a flexible substrate for applications in neural sensing and stimulation, particularly for μECoG (Micro-Electrocorticography) systems. While innovation in this area is expected to continue, the next set of challenges in expanding the application of GC MEMS involve the ability to build complex 3D origami-style structures using carbon as electrical and mechanical component, an approach similar to earlier 3D microprobes microfabricated using standard metal fabrication processes [9]. The origami-type technology presented in this research addresses this need and consists of microfabricating GC structures on high-temperature resisting substrates like

3

silicon, quartz or similar materials and then transferring the patterned devices on to a flexible

substrate like polyimide, and finally adding photolithographically patternable 2D layers that will

open up to form 3D structures. It has to be noted that while there are other reports of out-of-plane,

foldable MEMS devices, they often involve fabrication steps that are incompatible with the high

temperatures required for the pyrolysis of GC [10] and require stiff substrates [11]. Therefore, these

reported probes are not suitable for implantable neural electrodes and involve extremely precise and

time consuming manual manipulation [12, 13].

As a demonstration of this new technology, we present here a neural probe made of a

microelectrode array platform that integrates both surface (µECoG) and penetrating (intracortical)

GC electrodes onto a single flexible thin-film device. This is a natural extension, as GC has been

demonstrated to be a compelling platform for brain-computer interface (BCI) applications due to its

superior electrical and electrochemical properties and excellent surface chemistry that enables

enhanced adhesion to conductive polymers [8]. Along these lines, understanding how the brain

translates individual neural signals into behaviors, motivation and actions, requires the recording of

electrophysiological signals from large populations of neurons over multiple regions of the brain

[14]. While implantable microwires [15], tetrodes [16] and multiple electrode arrays (MEAs) [17]

are capable of sampling single-unit action potentials with high spatial and temporal resolution, the

implantation of the number of electrodes required to monitor such a large population of neurons

may not be feasible due to the possible damage to the brain tissue during implantation [18]. On the

other hand, ECoG arrays are capable of sampling from large neural populations as they are placed

on the surface of the brain, but do not provide the same spatial resolution as penetrating electrodes

[19]. MEMS fabrication technologies have been applied to ECoG arrays to address these

shortcomings and have led to improved data acquisition through an increase in electrode density

[20-22], improved electrode materials and fabrication techniques [22-24], and recordings of single

unit action potentials from subdural ECoG arrays [25]. Following these improvements, ECoG

arrays are becoming a platform of choice for BCI studies, mainly due to their ability to address

4

large areas of the cortex and support chronic implants owing to their reduced invasiveness [26-28].

Furthermore, these improvements in ECoG technology have motivated the further investigation of

the relationship between signals recorded from the brain surface and those generated by neurons

located at different levels of the cortex to fully exploit the potential of the ECoG platform. In fact,

research has already indicated a strong correlation between surface signals and the activity of

underlying neurons in the visual [29] and barrel [30] cortex in rats and in the primary

somatosensory [31] and primary motor [32] cortex in non-human primates.

Verification of this correlation between surface signals and the activity of the underlying

neurons requires the simultaneous recording of surface and intracortical signals. However, while

there has been significant research into ECoG array technology and in understanding the

relationship between ECoG signals and signals from underlying neurons, improving the technology

to simultaneously record these signals has been largely left unaddressed. Nearly all the

aforementioned electrophysiology experiments use separate systems to record the different

populations of neurons. Early experiments used single ball electrodes for ECoG recordings in

conjunction with a penetrating tetrode array [31]. Later, specialized ECoG arrays were developed

with multiple holes in the supporting substrate that allow the insertion of intracortical electrode

arrays through the ECoG device [29-32]; however, this approach still required fabrication,

placement and connection of multiple electrode systems. Some groups have developed integrated

electrode platforms to address these needs using either epoxy fixation of an intracortical MEA

through an ECoG array [29] or through specialized fabrication techniques to form SU8

microneedles on the surface of a thin-film electrode array [33-34]. However, both designs required

specialized fabrication techniques, with the former demanding that each device be individually

assembled, and thereby dramatically increasing both the fabrication time and variability between

the assembled devices. Furthermore, these designs introduce a new limitation, in that the

penetration depth of the intracortical MEA is set during device fabrication and assembly and,

therefore, cannot be adjusted during the implant surgery.

5

We submit that the new thin-film platform presented here, that combines both intracortical and surface GC electrodes into a single device through origami-like unfolding of the substrate to 3D structure, addresses these needs. Such device can be batch-fabricated using recently developed pattern-transfer techniques [6] to incorporate GC electrodes, and has the advantage of being completely self-assembled. The device was initially fabricated in a 2D geometry that takes the final 3D from, when it is folded into a zero-insertion force (ZIF) connector. In this report, we demonstrate the ability to fabricate 3D platforms with varying geometries and multiple penetrating arrays. We also verify the ability of the traces to maintain their connectivity when folded into 3D form by electrochemical characterization. To verify *in vivo* performance of our platform, we fabricated a device consisting of single penetrating array with several microelectrodes flanked by two µECoG arrays with a spring like system that allows the intracortical array to be inserted to varying depths without change to the µECoG electrode placements. As PEDOT coatings are useful to guarantee low impedance and ideal electrode conductivity of miniaturized electrodes [33], we coated the 30 µm diameter GC microelectrodes with PEDOT-PSS, reinforced with CNTs, which further improve mechanical and electrical properties [35-39]. Following fabrication, we performed an *in vivo* validation of the device by recording neural activity from the vibrissae representation of the rat primary somatosensory cortex (S1), namely the barrel cortex, leveraging the well-known cytoarchitecture and the physiology of this region [40-43].

2. Materials and Methods

In this section, we discuss the design of origami-style polymeric substrate supported GC MEMS neural probes, their microfabrication, and characterizations.

2.1 Microfabrication GC Microelectrode Arrays

The basic core fabrication method for the pattern transfer of a GC microelectrode array on a polyimide substrate is described in detail elsewhere [6-8]. Here, we extend the technology by adding a new reinforcing layer that is selectively deposited and patterned at areas of interest that allow a 3D origami-style unfurling. This modified process is summarized in Figure 1.

6

The microfabrication process starts with spin-coating SU8 negative photoresist (Microchem, MA) at 1000 rpm for 60 sec and soft-baking at 65°C for 10 min and 95°C for 30 min followed by UV exposure at ~400 mJ/cm^2. Post-exposure bake consists of 65°C for 1 min and 95°C for 10 min. This was followed by development of SU8 for 3-5 mins and curing at 150°C for 30 mins. Pyrolysis (1000°C in an inert N_2 environment) of the negative resist layer follows protocols described elsewhere [6-8]. After pyrolysis step, 6μm layer of photo-patternable polyimide (HD 4100) (HD Microsystems) was spin-coated on top of GC microelectrodes at 2500 rpms for 45 seconds, soft baked at 90°C for 3 min and at 120°C for 3 min, then cooled down to room temperature, and patterned through UV exposure at ~400 mJ/cm^2. Post-exposure bake consisted of 80°C for 1 min. Development was performed using a spry-puddle process where QZ3501 (Fuji Film) was dispersed to form a puddle on a stationary wafer. Rinse was applied after a set time of 15 sec, followed by spin-drying of the wafer (2000 rpms for 15 sec and 500 rpm/s ramp). The cycle was repeated 3 times and then the wafer was rinsed with SU8 developer (MicroChem). Subsequently, the polyimide layer was partial cured at 300°C for 60 mins under N_2 environment.

Following this, metal traces were deposited using NR9-1000PY negative photoresist (Futurrex) as a sacrificial layer. Futurrex was spin coated at 500 rpms for 45 seconds and ramped down for 10 seconds, then prebaked for 2 min at 150°C followed by 380 mJ/cm^2 UV exposure. Post exposure bake was done at 100°C for 2 minutes and sample was developed in pure RD6 developer (Futurrex Inc.) for 3 seconds. Subsequently, 20 nm chromium adhesion layer and 200 nm gold layer were deposited through sputtering. After metal deposition, a lift-off process was performed and the sacrificial layer was removed in acetone. To electrically insulate the device, 6μm of polyimide HD4100 (300 rpms) was spun, patterned (400 mJ/cm^2) and cured (350°C for 90 mins under N_2 environment). An additional thicker layer (30μm) of polyimide (Durimide 7520) (Fuji Film) that eventually becomes 3D structure was spin-coated (800 rpm, 45 s) and then patterned (400 mJ/cm^2) on top of the insulation layer to selectively reinforce the penetrating portion of the device. Then it was developed, as previously described, and final cured at 350°C for 90 minutes.

7

Subsequently, the device was released from the wafer through selective etching of silicon dioxide with buffered hydrofluoric acid. The device was assembled into the final 3D form and held in place by inserting both ends of the device into a custom PCB that served as the connector to the electrophysiological recording system. Representative images of devices after being released from the carrying wafer in their 2D form and of the origami-styled unfurled device assembled into connecting PCB in their 3D conformation are shown in Figures 2 and 4.
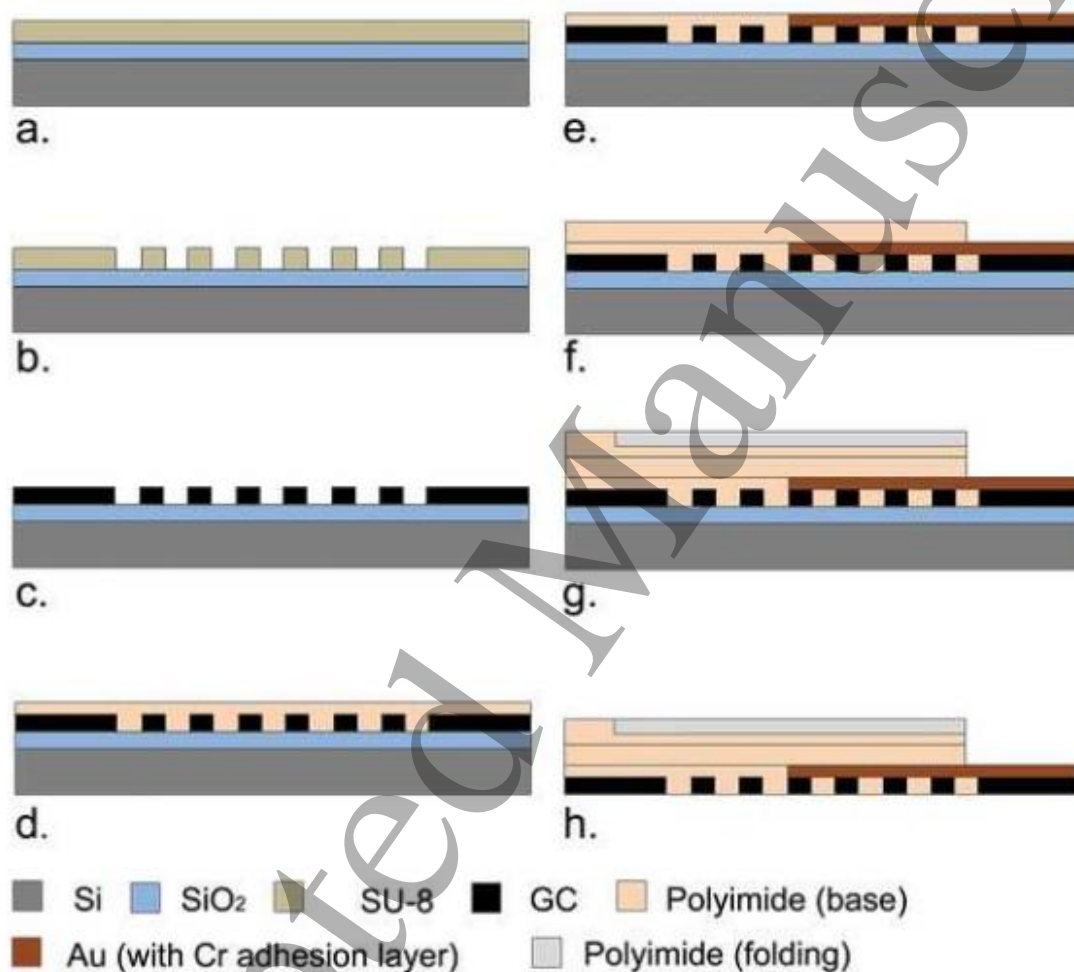
Figure 1. MEMS process for fabricating the multi-layered thin-film GC electrodes: a. Spin-coat negative photoresist (SU-8); b. Pattern SU-8 through lithography; c. Pyrolysis; d. Spin-coat and pattern polyimide base layer; e. Metal deposition and lift-off for traces and bump-pads; f. Spin-coat and pattern the polyimide insulation layer to get bump-pads access; g. Spin-coat and pattern the polyimide folding layer (Durimide 7520); h. Etch SiO_2 with BOE to release device from wafer.

8

2.2 Design of GC MEMS Origami Structures – Example of 3D GC Microelectrode Array

To demonstrate the versatility of the new architecture and modified pattern transfer technology introduced here, we highlight the device design of a portfolio of origami-type 3D probe structures. The devices were initially designed in a 2D geometry that could be batch-fabricated on a carrying wafer and when released, folded, and inserted into a ZIF connector would take on 3D form (Figure 2 and 3). The 2D geometry consisted of a series of cut-outs that, when folded, allowed the penetrating portions of the device to remain "in-plane," while the folded areas formed the ECoG portion of the device. Figure 2 shows a portfolio of such devices with (i) single or multiple shanks that unfurl from a 2D configuration to a 3D form and (ii) flat and foldable flaps that support the structure and contain pads for electrical connections. The combination of such geometries allows probes to assume a wide variety of conformations, and hence applications. It should be stressed that the flaps that contain surface microelectrodes were patterned from polyimide (HD4100) whereas the shanks that form penetrating microelectrode array were typically patterned from thicker polyimide, Durimide 7520.

Figure 3 shows a schematic of the device folding. Due to the cut-outs in the 2D geometry, when the device is folded upon itself, the penetrating portion of the device does not experience this backward force, and therefore remains in-plane, while the bulk of the device is folded back upon itself, and thereby forms the out-of-plane, 3D geometry of the ECoG portion. An additional layer of thicker polyimide (Durimide 7520) was patterned over the penetrating shanks to increase their mechanical robustness during 3D unfurling and allow penetration through the cortical tissue without the need for a penetration aid. The thickness of the layer of polyimide was determined by comparing the force required to penetrate the cerebral cortex of the rat, ~1.5 mN with the dura mater removed [44], to the critical buckling load of the penetrating shank calculated using the formula for Euler's critical load given below,

$$P_{cr} = (\pi^2\,EI)/(KL)^2$$

where Pcr is Euler's critical load, E is the Young's modulus of the material, I is the area moment of

9

inertia, K is the column effective length factor and L is the length of the column. The critical loads

for the penetrating portions of the different designs is given in Table 1.

Device	Width	Height	Length	Young's Modulus	Critical Load
Figure 2 B/C	1 mm	30 μm	2.5 mm	2.5 GPa [45]	8.8 mN
Figure 2 D	1 mm	30 μm	3.5 mm	2.5 GPa [45]	4.53 mN
Figure 4	1 mm	30 μm	5.7 mm	2.5 GPa [45]	1.7 mN

Table 1. Critical buckling load calculation for the penetrating portions of the different probe designs.

As the thicker layer of polyimide was only patterned over the penetrating shanks, the ECoG portion

of the device would remain ultra-flexible to promote contact between the electrodes and the surface

of the brain. Alternatively, a single foldable flap platform (Figure 2D) was designed for chronic

implantations in free moving animals, where disconnections between the ZIF connector and the

device pose a greater concern. The ultra-flexible flap containing the ECoG electrodes can be simply

held away from the penetration site using tether or forceps and following the implantation of the

penetrating portion be allowed to fall back into contact with the cortex.

Assessment of the biocompatibility of the specific polyimide used (Polyimide HD4100 and

Durimide 7520) for implantable medical device use, along with their suitability for peripheral nerve

and cortical implants and epiretinal stimulation, has been reported in earlier studies (46-51).

2.3 Assembly of GC MEMS Origami Structure

To validate the patterning technology, we chose to fabricate a single-shank penetrating array

as seen in Figure 4 specifically designed for an acute *in vivo* validation study in a rat. The curved

conformation the μECoG array substrate assumes when folded into its 3D form acts as a spring-like

structure that allows the penetrating array to be inserted at varying depths, while the parts of

μECoG array made of polyimide remains stationary. For this study, the device was designed to

record from the barrel cortex in rats. The electrodes in both arrays are 30μm in diameter and have a

center to center pitch of 300μm in the intracortical array and 500μm for the μECoG array. The

10

intracortical array contains five electrodes stacked vertically, with the deepest electrode reaching a depth at least 2.3mm. A detailed schematic of the device, reporting the overall dimensions, diameter of the electrodes and center to center distance is provided in Supplementary Figure 1. This penetration depth and electrode spacing allows the device to record signals from at least one electrode for each cortical layer (from layer II to layer V). The µECoG array contains additional six microelectrodes (three on each side of the intracortical array) to allow comparison of surface recordings at different locations with depth recordings through the cortex.
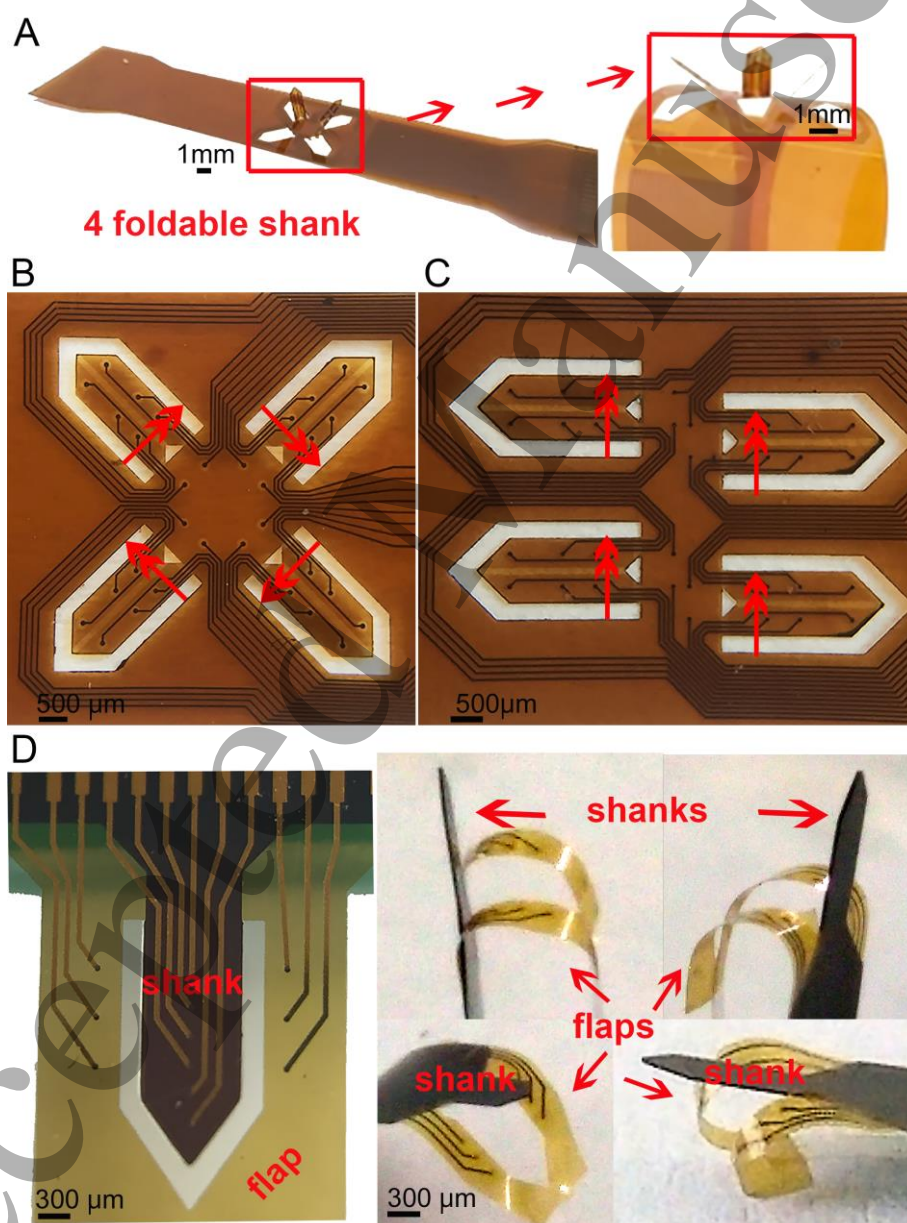

Figure 2. Origami MEMS Portfolio. (A) and (B) Four-shanks origami probes. (B) and (C) Magnifications of two possible probe designs (D) Single-shank origami probe with foldable flap.
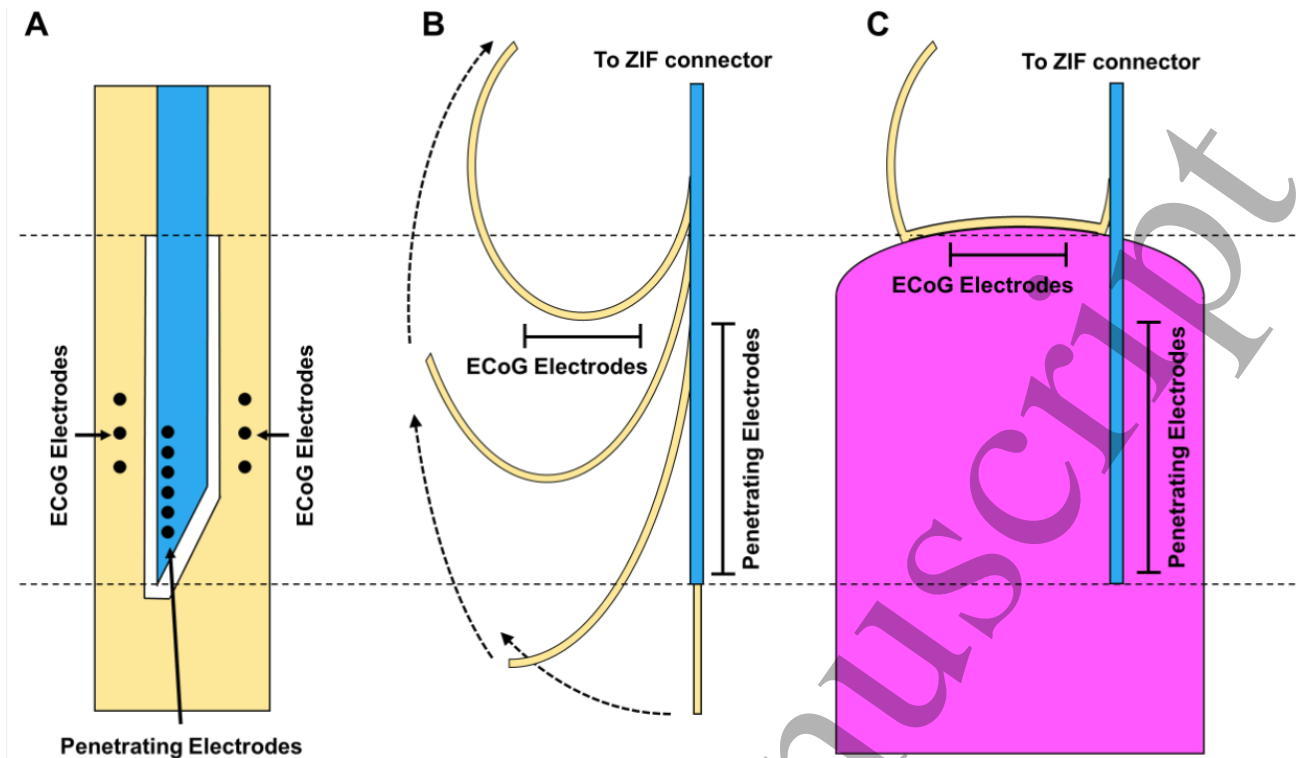
11

Figure 3. Schematic of the folding process and implantation of a 3D integrated intracortical and epicortical neural probe. (A) Overhead schematic of the device immediately following release from the wafer. (B) Schematic of the device folding to the final 3D form by the insertion of both ends into the ZIF connector. Due to the 2D geometry of the device, the penetrating portion is not subjected to the force back towards the ZIF connector, and therefore remains in-plane, while the ECoG electrodes are folded back towards the connector creating the 3D structure. (C) Schematic of the device implanted in the cortex of a rat. Due to the ultra-flexibility of the ECoG portion, the device is able to follow the surface of the cortex, promoting contact between the electrodes and the surface of the brain. The probe is able to bend through almost 180° angle, if needed.

2.4 PEDOT-PSS-CNT electrochemical deposition

Poly(3,4-ethylenedioxythiophene) (PEDOT) and carboxylated MWCNTs (COOH-CNTs, NC 3151, < 4 % of COOH functional groups, Nanocyl S.A., Belgium) nanocomposites (PEDOT-CNT) were co-electrodeposited from a 0.5 M 3,4-ethylenedioxythiophene (EDOT, Sigma-Aldrich, USA) aqueous solution containing 1 mg/ml of suspended COOH-CNTs and 0.6 wt% of poly(sodium 4-styrenesulfonate) (PSS) (Sigma-Aldrich, USA). COOH-CNTs were suspended in ultrapure water

12

(Milli-Q, Millipore, USA) by horn sonication (Vibra-Cell VCX130, Sonics and Materials, USA) (6

s at 66% duty cycle pulses, 4 W/ml) for 30 min while keeping the solution cooled with an ice bath.

PSS and the monomer were added to the suspension immediately afterwards, and the solution was

kept deoxygenated by bubbling nitrogen. The electrochemical deposition was carried out using a

polymerization potential of 0.8 V vs. reference electrode for 10 CV cycles. Depositions were

carried out using a potentiostat/galvanostat (PARSTAT 2273, Princeton Applied Research, USA)

connected to a three-electrode electrochemical cell with a platinum counter electrode and an

Ag/AgCl reference electrode.

2.5 Device Characterization

Once the devices were assembled in 3D fashion, the electrochemical characterization of the devices

was carried out in 0.9% NaCl aqueous solution through electrochemical impedance spectroscopy

(EIS). EIS measurements were performed by superimposing a sine wave (10 mV RMS amplitude)

onto the open circuit potential, in the frequency range from 1 to 10^5 Hz. EIS were carried out using

a potentiostat/galvanostat (Reference 600, Gamry Instruments, USA) connected to a three-electrode

electrochemical cell with a Pt counter electrode and a Ag|AgCl|KCl (sat.) reference electrode.

The capacitive charging ability of the PEDOT-PSS-CNT coated GC microelectrodes was evaluated

by cyclic voltammetry (CV) and voltage transient in a physiological aqueous solution (NaCl 0.9%).

For CVs, the potential on the working electrode was swept between 0.8 and -0.6 V vs Ag/AgCl at a

scan rate of 100 mV/s, starting at open-circuit potential and sweeping in the positive direction first.

The Charge Transfer Capacities (CTC) were calculated as the time-integral of an entire CV cycle

between 0.5 and −0.5 V, or between -0.6 and 0.8 V (CTC_2). For voltage transient, a cathodic-first

charge-balanced biphasic symmetric current pulse with 400 μs cathodic half-phase period was used.

The charge injection limit, defined as the maximum quantity of charge an electrode can inject

before reaching the water electrolysis potential, was calculated as the time integral of the current in

the loading phase normalized by the geometric area of the microelectrode.

13

2.6 In-vivo Test

The device with GC microelectrodes coated with PEDOT-PSS-CNT was *in-vivo* validated. The

surgical procedures were performed on one Long-Evans male rat (weight 400g). The experimental

plan was designed in compliance with the guidelines established by the European Communities

Council (Directive 2010/63/EU, Italian Legislative Decree n. 26, 4/3/2014) and the protocol was

approved by the Ethics Committee for animal research of the University of Ferrara and by the

Italian Ministry of Health (authorization n° 332/2015-PR). The animal was anesthetized with a

mixture of Zoletil (30mg/kg) and Xylazine (5 mg/kg) delivered intraperitoneally. The depth of

anesthesia was monitored for the entire duration of the experimental session by testing the absence

of hindlimb withdrawal reflex and was maintained by additional doses of anesthetic (i.m.). Under

anesthesia, the animal was placed on stereotaxic apparatus (David Kopf Instruments, USA) and an

incision of 2 cm was made along the midline of the cranium. The underlying muscle and connective

tissue were retracted to expose the skull and a craniotomy of 5x5 mm was made on the parietal bone

to expose the primary somatosensory cortex (S1) [52].

To record the intracortical neural activity, the shaft was lowered into the vibrissa region of S1 (A-P

coordinates between −1.5 and −5.0 mm and M-L coordinates between 3.5 and 5.5 mm) at the

maximum depth of 2 mm to enable the 5 penetrating electrodes acquire signals from the different

layers of the cortex. To test the recording capability of the 6 surface electrodes, somatosensory

evoked potentials (SEP) were elicited through mechanical whiskers stimulation (see below). Eight

25 min sessions of evoked activity and two 10 min of spontaneous activity were recorded. To elicit

neural activity, a vibrating system was used to produce a multi-whiskers deflection along the

horizontal plane. Three different mechanical stimulation patterns were used. The whiskers,

contralateral to the recorded cortex, were cut 1 cm from the base and included in a Velcro strip

attached to a rod moved by a shaker (Type 4810 mini shaker; Bruel & Kjaer) controlled by a

National Instruments board (Austin, TX, USA). The deflection stimulus consisted of 10 trains of 10

truncated Gaussians of 12 ms duration at 9 Hz followed by a 5 sec pause. The amplitude of the

stimulus was changed after each train to obtain multi-whiskers deflections respectively of 250, 500, and 800 μm. Each train of the different amplitude was repeated 20 times with 60 seconds pause between cycles.

Electrophysiological data were acquired using a TDT multi-channel recording system 3 (Tucker Davis Technologies, USA) including ZIF-Clip® head-stage with unity (1x) gain, RZ2 real-time processor and PZ2-256 battery-powered preamplifier. Data was digitized at a sample rate of 24,414 samples/s (18-bit resolution) and transferred from RZ2 to the PC by fast fiber optic connection. Evoked and spontaneous activity data were thus stored on a PC for the subsequent offline analysis.

To analyze the recording performance of the 5 penetrating electrodes, the signal-to-noise ratio (SNR) was computed on the high frequency components of the signal. SNR was calculated as peak-to-peak amplitude of the mean waveform detected, divided by twice the standard deviation (σ) of the noise.

For each penetration, the signal was digitally high-pass filtered (Butterworth, 4-poles) above 250 Hz and the waveform discrimination was performed at a voltage threshold of 2 times the root-mean square voltage of the background noise. The signal amplitude was taken as the mean peak-to-peak amplitude of the waveform detected and the σ Noise was the standard deviation of the data stream after all waveforms have been removed. The Off-Line Sorter software (Plexon Inc, USA) on the continuous traces was used.

To extract the SEPs from the surface, the signal was down-sampled at 3051.8 Hz and digitally low-pass filtered (Butterworth 2nd order) below 300 Hz using MATLAB software (Mathworks, USA). The evoked responses for each amplitude of whiskers deflection were averaged from 0 to 100 ms after trigger pulses using EEGLAB MATLAB toolbox and OriginPro (OriginLab, USA).

3. Results

3.1 GC MEMS Origami Structure

We were able to design and fabricate a platform that incorporated GC electrodes into a 3D thin-film flexible substrate that is capable of recording both epicortical and intracortical electrophysiological

15

signals in a robust and reproducible manner. Additionally, the platform is compatible with a number

of different device geometries and can be tailored to the electrophysiological study of particular

interest. Folding and assembly of the different devices was accomplished in the same step and

simply involved inserting both ends of the device into the ZIF clip of the PCB (Figure 4B). The two

ends of the device were designed to fit snugly into the connector (< 200μm difference between the

width of the device and connector) and the device folding could be done quickly and repeatedly.

Alternatively, for devices with a smaller footprint (Figures 2 and 4), the 3D form came about

naturally when inserting the device into an agar phantom. The insulating polyimide layers around

the μECoG arrays had a total thickness of approximately 8μm allowing them to be ultra-flexible

and conform to the surface of the brain. The addition of a 30μm thick polyimide layer (that appears

dark in appearance in Figures 2D, 4A & B) over the penetrating array, increased the stiffness of the

penetrating portion of the device, allowing it to penetrate both the cortical tissue and dura.

PEDOT-PSS-CNT composite was successfully polymerized on the 30μm diameter microelectrodes

with very high localized precision, as can be seen from a representative picture of a PEDOT-PSS-

CNT coated GC microelectrodes (Figure 5B). A High-resolution SEM image of the PEDOT-PSS-

CNT layer shown in Figure 5C demonstrates a very porous morphology from which emerges a fine

nanoscale CNT scaffold structure, similar to what was reported in a previous study on flat and

spherical Au electrode surfaces [53-54]. As expected, after the deposition of the PEDOT-PSS-CNT

composite, there was a significant reduction in the impedance (nearly three orders of magnitude at 1

kHz) of the electrodes (Figure 6A), from 555.1±128.1 kΩ to 3.6±1.2 kΩ at 1kHz. The impedance of

the PEDOT-PSS-CNT coated μECoG GC microelectrodes before and after folding remain constant

(4.2 ±0.7 kΩ at 1kHz). This indicates that the folding of the device does not damage the gold traces

or the GC electrodes. EIS plots are reported in Supporting Figure S3 of Supplementary Information.

The PEDOT-PSS-CNT coated GC microelectrodes present CTC_{tot} of 300 mC/cm^2 in the -0.5/0.5 V

EW and of 458 mC/cm^2 the -0.6/0.8 V EW. The experimentally verified charge injection limit

(Q_{inj}) is 7.2 mC/cm^2. These results are comparable to previously reported CTCs and charge

16

injection limit of PEDOT-PSS-CNT coated nanostructured gold microelectrodes [54-55]. An

example of CVs of PEDOT-PSS-CNT coated GC microelectrodes with two different

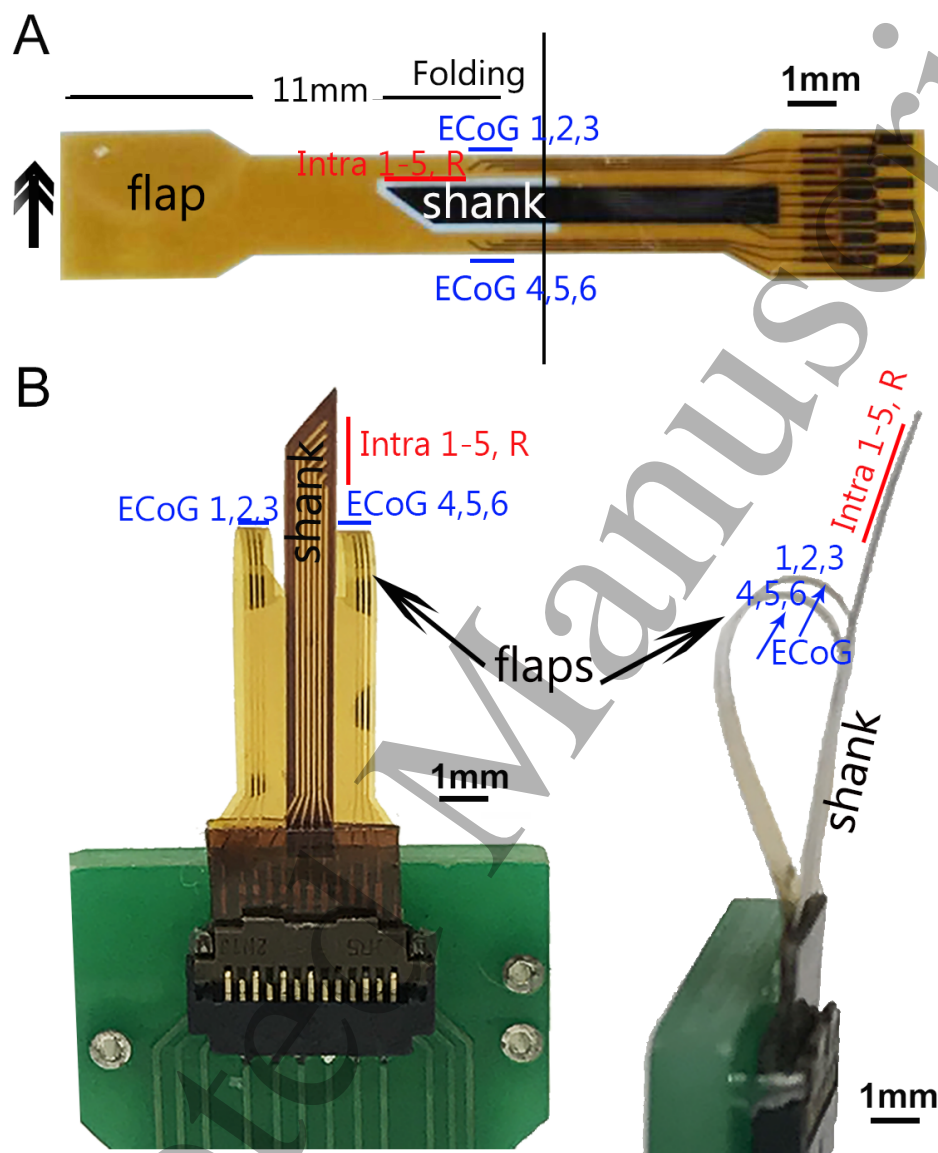electrochemical windows (EW) is shown in Supporting Figure S2 of Supplementary Information.

Figure 4. (A) Single-probe origami (Epi-Intra) device after being released from the carrying wafer in its 2D

form; (B) Representative images of the Epi-Intra folded device assembled into the connecting PCB in its 3D
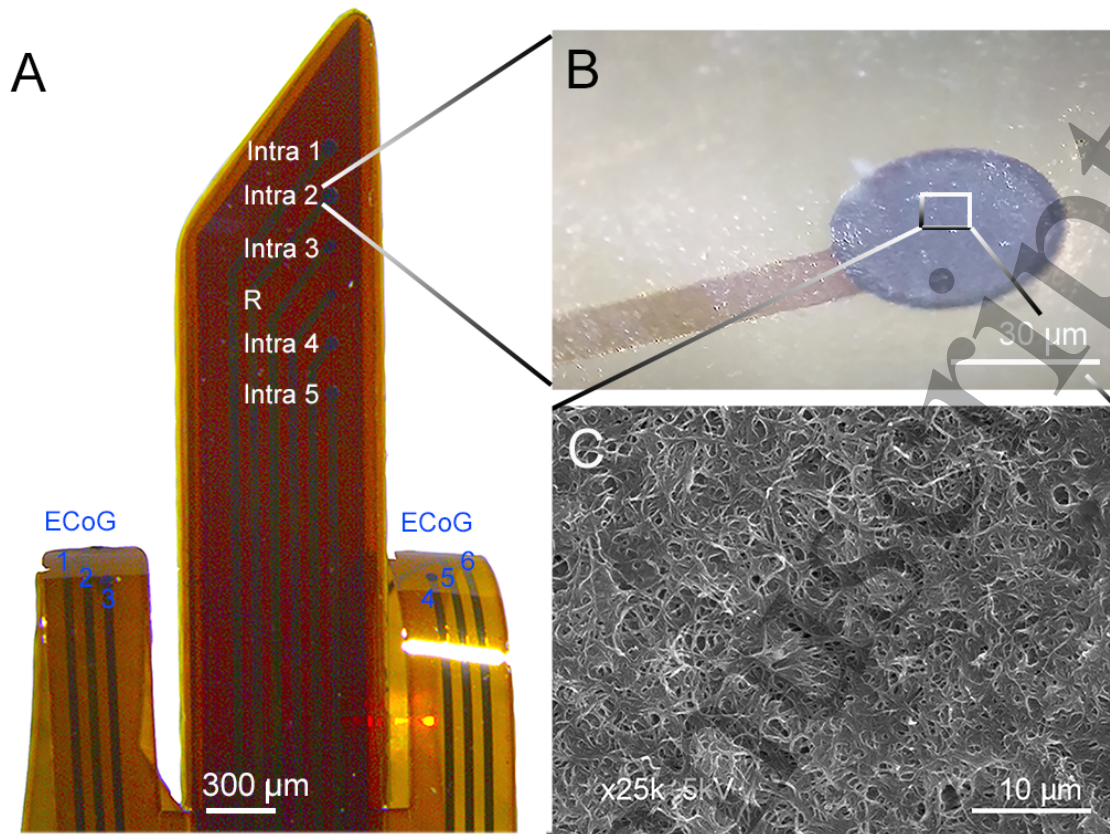
conformation.

Figure 5. A. Magnification of Epi-Intra Device, B. Magnification of a PEDOT-PSS-CNT coated microelectrodes; C. SEM image of PEDOT-PSS-CNT morphology.

To validate its ability to penetrate the brain tissue and its functionality, the combined MEA was tested *in vivo* through acute intracortical and epicortical recording sessions in a rat model. The shaft of the device was able to penetrate the rat brain tissue and the two µECoG array areas adhered well to the brain surface without interfering with the intracortical part. After implanting the device, we did not observe significant change in impedance of the microelectrodes, which remained nearly identical to the impedance measured during preliminary *in vitro* tests, for both the intracortical and epicortical recording sites (3.6±1.2 kΩ at 1kHz before and 3.7±1.3 kΩ at 1kHz after). The impedance spectra of a representative PEDOT- PSS-CNT-coated electrode before and after an *in vivo* intracortical recording session are shown in Figure 6B.
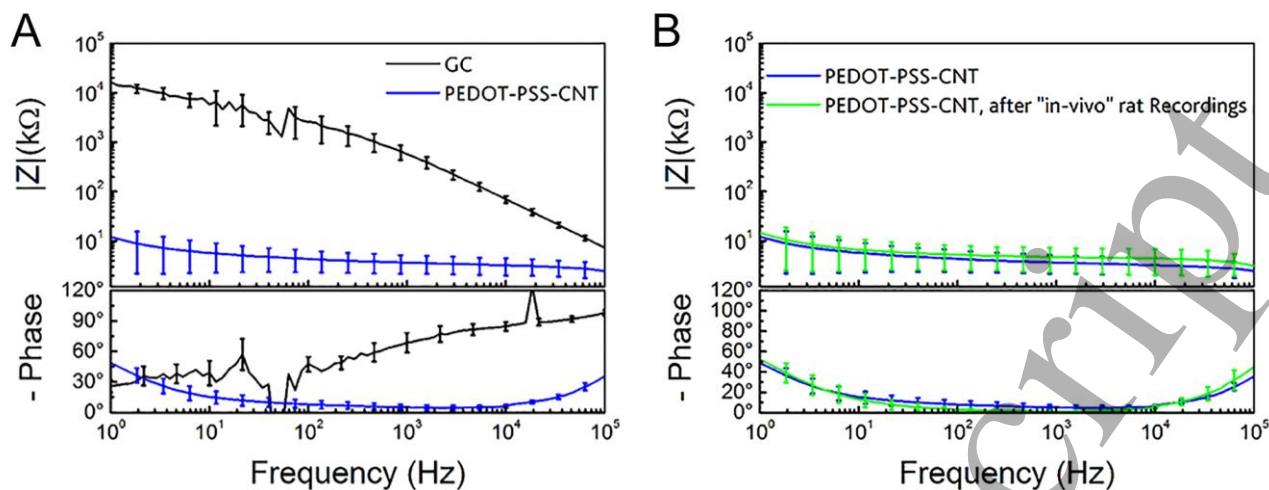
18

Figure 6. A. Impedance spectra (mean and deviation, n=12) of the 30μm diameter microelectrodes before (black) and after PEDOT-PSS-CNT (blue) deposition; B. Impedance spectra (mean and deviation, n=12) of the 30μm diameter PEDOT-PSS-CNT coated microelectrodes before (blue) and after (green) intra- and epi-cortical *in vivo* recordings in rat brain.

In vivo results are schematically summarized in Figure 7. The surface electrodes were able to record typical SEPs with amplitudes following those of whiskers deflection [56] (see Table 2). For the penetrating electrodes, the amplitude of recorded high frequency signals depends on their position, with smaller values detected by electrodes nearest to the surface and larger ones by the deeper electrodes, both for stimulated and spontaneous activity (see Table 3 and Figure 7). A similar trend was found for the mean value of SNR calculated for each channel both for spontaneous and for stimulated activity, as shown in Figure S3 (Supporting Information).

Surface Electrode (ECoG 1-6)			
Whiskers deflections (μm)	250	500	800
Peak-to-peak amplitude	258.61±52.73	248.53±56.81	273.25±48.85

Table 2: mean SEP amplitudes for 8 acquired traces under the 3 different whiskers stimulations (mean value μV ± SD)
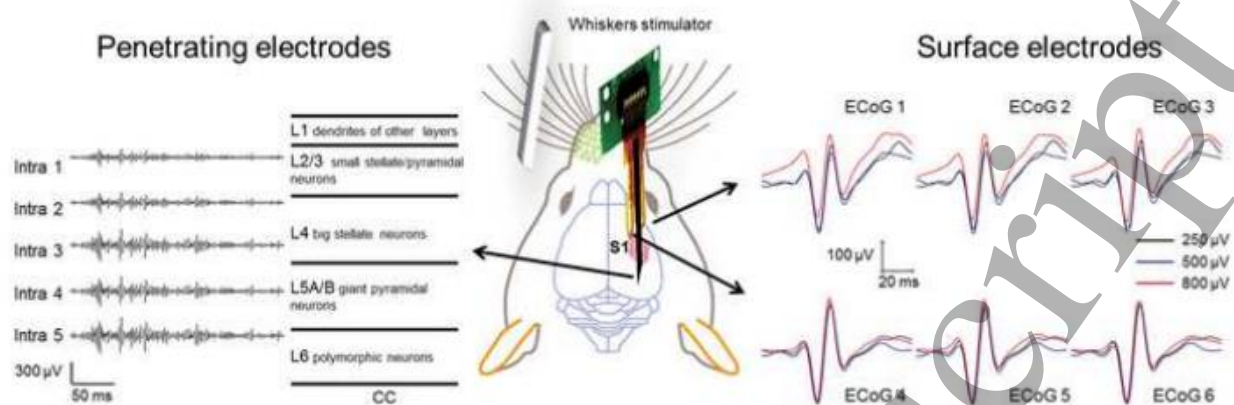
19

Figure 7. Schematic representation of a recording session on rat vibrissae region of S1. The whiskers pad, contralateral to the recorded cortex, was in contact with a flag to produce whiskers deflection at 3 different amplitudes (whiskers stimulator). The shaft of the device was inserted into the cortex perpendicularly to the surface, since each electrode was able to record neural signal. On the left side of the picture is shown an example of recorded traces from the 5 penetrating electrodes, from the most superficial layer with small signals (Intra 1,2), to the deepest (Intra 3,4,5) with large signal (scale bar 300 µV and 50 ms). In the figure, each trace was associated with the respective cortical layers and neuron populations during recording session. The six surface channels (ECoG 1-6) were coupled with the brain surface to record SEPs. In the right side, the small panels show an example of mean SEPs recorded after 20 cycles for each of the 3 amplitude deflections (scale bar100 µV and 20 ms). In black the SEPs elicited using a 250 μm whiskers deflection, in blue 500 μm and in red 800 μm.

Signal Amplitudes	Intra 1	Intra 2	Intra 3	Intra 4	Intra 5
Stimulated activity	851.9±153.7	871±159.6	995.1±280.1	1007.6±264.4	1097.7±421.7
Spontaneous activity	458.7±92.7	524.3±138.9	557.0±231.7	540.6±208.4	557.0±277.9

Table 3: Signal amplitudes for each 'intra'-cortical channel following eight whiskers stimulations and two recordings from spontaneous activity (mean value µV ± SD).

4. Discussion

The orgami-style 3D platform presented here, to the best of our knowledge, is the first combined epicortical and intracortical recording platform in which the electrode material, size and fabrication method are identical between the penetrating and surface electrodes. A challenge in creating such a hybrid device stems from the fact that the ideal mechanical properties for penetrating and μECoG arrays are different, most notably penetrating devices require a stiffer substrate to penetrate the tissue, while μECoG arrays need to remain ultra-flexible to better conform to the brain surface. Therefore, for many combined epicortical and intracortical recording set-ups, the penetrating and μECoG recording arrays are fabricated using different materials and methods, and as a result the electrode material and geometries are not consistent between the epi and intracortical arrays [30-32, 34-35]. This makes direct comparison between the acquired signals more difficult as the differences in the electrodes must be taken into account. Our platform employed the same fabrication method for both the epicortical and intracortical arrays, and therefore the electrodes were consistent across both portions of the device. Polyimide was chosen as the substrate material due to its mechanical and insulating properties and its ability to be deposited at significantly different thicknesses based on its initial viscosity and spin-coating speed. By varying the thickness of the polyimide layers over the μECoG and penetrating arrays, we were able to tune the mechanical properties of the different portions of the device. Particularly, polyimide HD-4100 was used as insulator layer for the foldable segment of the device because of its excellent mechanical properties and excellent resistance to thermal and chemical extremes. Durimide 7520 was added as a thickening layer of the penetrating shank because it allows for a cured film thickness up to 50μm. Additionally, it presents superior mechanical property retention after extended pressure cooker test (> 1000 hour) and excellent adhesion.

As can be seen in Figures 2 and 3, we are able to fabricate a variety of geometries depending on the electrophysiological study. In the example used to validate the platform (Figure 3), the μECoG arrays were arranged on a slight convex curve. This arrangement was beneficial in two ways: (1) it

21

improved the contact between the μECoG electrodes and cortical surface and (2) it acted like a small spring, allowing the penetrating portion of the device to be inserted at varying depths without disturbing the position of the μECoG electrodes. Unlike other examples of combined epicortical and intracortical MEAs where the vertical distance between the penetrating and intracortical electrodes are fixed once the device is fabricated [33-35], the distance between the two sets of electrodes of this device can be altered during the implant surgery. Therefore, the reported design is less impacted by any variations between devices caused by fabrication or assembly, as the penetration depth is independent of μECoG portion of the device and can be used for multiple experiments where different penetration depths may be required. As the platform is fabricated from the thin-film, flexible polymer polyimide, it lends itself well to chronic applications where large mechanical mismatches between the device and brain tissue may lead to chronic inflammation, the formation of a glial scar and loss of device function [6]. In addition, the fact that the epicortical and intracortical arrays are integrated on a single device with one connector makes this device well suited for chronic applications by reducing the number of connections required.

Furthermore, PEDOT-PSS-CNT coatings drastically decreased the impedance of the 30μm diameter μECoG and intracortical microelectrodes, guaranteeing an ideal electrode conductivity of miniaturized electrodes [32]. Both cortical and intracortical recordings would greatly benefit from reduction of the impedance of recording sites. In fact, a low impedance is fundamental to enhance the signal recording quality, reduce the background noise, and, consequently, increase the signal-to-noise ratio [55]. At the same time, a lower impedance with no dimensional increase enables the injection of relatively large capacitive currents whilst minimizing electrode degradation due to Faradaic effects, as reported in our previous study on similar PEDOT-PSS coated GC microelectrodes [8]. We used electrochemical deposition because it can be performed at room temperature and applied to an unconstraint variety of materials. We adopted GC as microelectrode material for its superior electrochemical properties and PEDOT-PSS because of its high conductivity and chemical stability. Further, a combination of GC and PEDOT-PSS offers an

22

excellent adhesion better than Pt and PEDOT-PSS, as previously reported [8]. In particular, we reinforced PEDOT-PSS with CNTs because PEDOT-CNT composite outperforms plain PEDOT in terms of impedance reduction, effective surface area increase, conductivity, and mechanical stability, taking advantage of the excellent properties of CNTs [36-39]. In fact, our study confirmed that PEDOT-PSS-CNT composites remain attached to the GC microelectrodes before and after folding as well as after implantation, as supported by the impedance measurements that showed no noticeable changes (Figure 6B and Supplementary Figure S3).

In summary, the recently introduces technologies [6-8] that allow for pattern transfer and the integration of GC electrodes into thin-film polymeric substrates allow us to exploit: (1) GC as microelectrode substrate, (2) flexible polymer polyimide as substrate. This provides a great advantage even compared to the state-of-the-art silicon MEMS technology, which allows to produce smaller devices, with precise and highly reproducible mechanical and geometric characteristics, but still using metal microelectrodes and a rigid substrate.

Lastly, the *in vivo* test has shown that the device was able to record neural signals with a high sensitivity to the physiology of the specific cortex region where the electrodes were placed (i.e. the vibrissae region of S1). For ECoG, response to variations of whiskers deflection amplitude was excellent, while for the penetrating electrodes, waveform amplitudes of recorded high frequency are in good agreement with the anatomical characteristics of the neuronal population following the laminar structure of the primary somatosensory cortex [40-43].

5. Conclusions

In this study, we introduced a new microfabrication and pattern transfer technology that allows origami-style 3D glassy carbon MEMS (GC MEMS) structures supported on flexible polymeric substrates. These devices demonstrate the versatility of the technology, delivering a flexible, thin-film multipurpose platform that contains both surface (ECoG) and penetrating (intracortical) GC MEAs on a 3D device. The device can be batch-fabricated and is easily reproducible using pattern-

transfer techniques. The platform can be fabricated in a variety of geometries and incorporates GC microelectrodes coated with PEDOT-PSS-CNT to achieve low impedance of the miniaturized electrodes. We tested the manufactured device *in vivo* to confirm that the shank was able to penetrate the brain tissue without buckling and that the μECoG arrays could adhere to the cortex without damaging it or interfering with the penetrating portion. We additionally validated the ability of the device to record neural activity from the vibrissae representation of the rat primary somatosensory cortex (S1). From the physiological point of view, the advantage of this platform is that the surface and penetrating electrode contact sites are equal in design, size and material, allowing a much more reliable comparison between signals acquired epidurally and intracortically. In addition, the compact and simple design makes it suitable for chronic implants and long-term electrophysiological studies. In conclusion, the innovative platform presented here demonstrates that there is significant potential for GC-based thin-film technology to successfully interface with the brain in different configurations simultaneously from a single flexible sheet of polymeric substrate. Furthermore, we expect foreign body response to our thin and flexible integrated device during long-term implants to be less severe than the one arising after implanting stiff penetrating probes.

Conflict of Interest Statement

The authors declare that the research was conducted in the absence of any commercial or financial relationships that could be construed as a potential conflict of interest.

Supplementary information

24

References

1. R. L. McCreery, "*Advanced Carbon Electrode Materials for Molecular Electrochemistry*", *Chem. Rev.*, 2008, *108* (7), pp 2646–2687, DOI: 10.1021/cr068076m, 2008.

2. O. J. A. Schueller, S. T. Brittain, C. Marzolin, and G. M. Whitesides, "*Fabrication and characterization of glassy carbon MEMS,*" Chem. Mater., vol. 9, pp. 1399–1406, 1997.

3. Kassegne, S., Moon, K., Martín-Ramos, P., Majzoub, M., Ozturk, G., Desai, K., Parikh, M., *et al.* "*Organic MEMS/NEMS-based High-Efficiency 3D ITO-less Flexible Photovoltaic Cells*", JMM (Journal of Micromechanics and Microengineering), 22 (11), 115015, 2012.

4. Wang, C., Jia, G., Taherabadi, L.H., Madou, M.J., "*A novel method for the fabrication of high-aspect ratio C-MEMS structures*", Journal of microelectromechanical systems, 2005.

5. Ranganathan, S., McCreey, R., Majji, S.M., Madou, M., "*Photoresist-derived Carbon for Microelectromechanical Systems and Electrochemical Applications*", J Electrochem Soc, 147 (2000), pp. 277–282

6. M. Vomero, P. van Niekerk, V. Nguyen, N. Gong, M. Hirabayashi, A. Cinopri, K. Logan, A. Moghadasi, P. Varma, S, Kassegne, *A novel pattern transfer technique for mounting glassy carbon microelectrodes on polymeric flexible substrates*, Journal of Micromechanics and Microengineering 2016; 26: 025018. Doi:10.1088/0960-1317/26/2/025018.

7. S. Kassegne, M. Vomero, R. Gaguglio, M. Hirabayashi, E. Özyilmaz, S. Nguyen, J. Rodriguez, E. Özyilmaz, P. van Niekerk, A. Khosla, *Electrical impedance, electrochemistry, mechanical stiffness, and hardness tunability in glassy carbon MEMS μECoG electrodes*. Microelectronic Engineering 133 (2015) 36-44. http://dx.doi.org/10.1016/j.mee.2014.11.013

8. M. Vomero, E. Castagnola, F. Ciarpella, E. Maggiolini, N. Goshi, E. Zucchini, S. Carli, L. Fadiga, S. Kassegne, D. Ricci, *Highly Stable Glassy Carbon Interfaces for Long-Term Neural Stimulation and Low-Noise Recording of Brain Activity*, Nature Sci. Rep 7 (2017) 40332. doi: *10.1038/srep40332.*

9. S. Takeuchi, T. Suzuki, K. Mabuchi and H. Fujita *3D flexible multichannel neural probe array*

J. Micromech, Microeng. 14 (2004) 104–107.

10. J. P. Whitney, P. S. Sreetharan, K. Y. Ma, R. J. Wood, *Pop-up book MEMS,* Journal of Micromechanics and Microengineering 21(11) (2011): 115021.

11. S. A. Zotov, M. C. Rivers, A. A. Trusov, A. M. Shkel, *Folded MEMS pyramid inertial measurement unit*, IEEE Sensors Journal 11(11) (2011) 2780-2789.

12. E. E. Hui, R. T. Howe, M. S.Rodgers. *Single-step assembly of complex 3-D microstructures. Micro Electro Mechanical Systems, 2000. MEMS 2000. The Thirteenth Annual International Conference on*, pp. 602-607.

13. A. C. Siegel, D. A. Bruzewicz, D. B. Weibel, G. M. Whitesides. *Microsolidics: fabrication of three dimensional metallic microstructures in poly (dimethylsiloxane)*. Advanced Materials 19(5) (2007): 727-733.

14. G. Buzsáki, Large-scale recording of neuronal ensembles, *Nature neuroscience* 7 (2004) 446-451. doi:10.1038/nn1233

15. C. Palmer, *A microwire technique for recording single neurons in unrestrained animals*, *Brain research bulletin* 3 (1978) 285-289. http://dx.doi.org/10.1016/0361-9230(78)90129-6

16. C.M. Gray, P.E. Maldonado, M. Wilson, B. McNaughton, Tetrodes markedly improve the reliability and yield of multiple single-unit isolation from multi-unit recordings in cat striate cortex, *Journal of neuroscience methods* 63 (1995) 43-54. http://dx.doi.org/10.1016/0165-0270(95)00085-2

17. P. K. Campbell, K.E. Jones, R.J. Huber, K.W. Horch, R.A. Normann, A silicon-based, three-dimensional neural interface: manufacturing processes for an intracortical electrode array, IEEE Trans Biomed Eng. 38(1991) 758-768. doi: 10.1109/10.83588

18. V.S. Polikov, P.A. Tresco, W. M. Reichert, Response of brain tissue to chronically implanted neural electrodes, J Neurosci Methods. 148 (2005) 1-18. doi: 10.1016/j.jneumeth.2005.08.015

19. E.C. Leuthardt, G. Schalk, J.R. Wolpaw, J. G. Ojemann, D.W. Moran, A brain–computer interface using electrocorticographic signals in humans, J. Neural Eng. 1 (2004) 63 doi:

10.1088/1741-2560/1/2/001

20. B. Rubehn, C. Bosman, R. Oostenveld , P. Fries, T. Stieglitz, A MEMS-based flexible
    multichannel ECoG-electrode array, J Neural Eng. 6 (2009) 036003. DOI: 10.1088/1741-
    2560/6/3/036003

21. J. Viventi, D-H Kim, L. Vigeland, et al., Flexible, foldable, actively multiplexed, high-density
    electrode array for mapping brain activity *in vivo*, Nature neuroscience 14 (2011) 1599-1605.
    doi:10.1038/nn.2973

22. G. Hotson, D.P. McMullen, M. F. Fifer, M.S. Johannes, K.D. Katyal , M.P. Para, R. Armiger,
    W.S. Anderson, N.V. Thakor, B.A. Wester, N.E. Crone, Individual finger control of a modular
    prosthetic limb using high-density electrocorticography in a human subject, J. Neural Eng. 13
    (2016) 026017. doi: 10.1088/1741-2560/13/2/026017

23. E. Castagnola, L. Maiolo, E. Maggiolini, A. Minotti, M. Marrani, F. Maita, A. Pecora, G.N.
    Angotzi, A. Ansaldo, M. Boffini, L. Fadiga, G. Fortunato, D. Ricci, PEDOT-CNT-coated low-
    impedance, ultra-flexible, and brain-conformable µECoG arrays, IEEE Trans Neural Syst
    Rehabil Eng. 2015; 23: 342-350. Doi: 10.1109/TNSRE.2014.2342880

24. D. Khodagholy, T. Doublet, P. Quilichini, M. Gurfinkel, P. Leleux, A. Ghestem, E. Ismailova,
    T. Hervé, S. Sanaur, C. Bernard, G. G. Malliaras, In vivo recordings of brain activity using
    organic transistors, Nature communications 4 (2013); 4:1575. DOI: 10.1038/ncomms2573

25. D. Khodagholy, J.N. Gelinas, T. Thesen, W. Doyle, O. Devinsky, G.G. Malliaras, G. Buzsáki,
    NeuroGrid: recording action potentials from the surface of the brain, Nature neuroscience 18
    (2015) 310-315. doi:10.1038/nn.3905.

26. G. Schalk, E.C. Leuthardt, Brain-computer interfaces using electrocorticographic signals, IEEE
    Rev Biomed Eng. 4 (2011) 140-154. doi: 10.1109/RBME.2011.2172408.

27. A. Ritaccio, P. Brunner, M.C. Cervenka, N. Crone, C. Guger, E. Leuthardt, R. Oostenveld, W.
    Stacey, G. Schalk, Proceedings of the first international workshop on advances in
    electrocorticography, Epilepsy & Behavior 19 (2010) 204-215.

27

http://dx.doi.org/10.1016/j.yebeh.2010.08.028

28. A. Ritaccio, P. Brunnera, A. Gunduz, D. Hermes, L. J. Hirsch, J. Jacobs, K. Kamada, S. Kastner, R. T. Knight, R. P. Lesser, et al., Proceedings of the Fifth International Workshop on Advances in Electrocorticography. *Epilepsy & Behavior* 41 (2014) 183-192. http://dx.doi.org/10.1016/j.yebeh.2014.09.015

29. H. Toda, T. Suzuki, H. Sawahata, K. Majima, Y. Kamitani, I. Hasegawa, Simultaneous recording of ECoG and intracortical neuronal activity using a flexible multichannel electrode-mesh in visual cortex. Neuroimage 54 (2011) 203-212. doi: 10.1016/j.neuroimage.2010.08.003.

30. H. Watanabe, T. Sakatani, T. Suzuki, M.A. Sato, Y. Nishimura, A. Nambu, M. Kawato , T. Isa, Reconstruction of intracortical whisker-evoked local field potential from electrocorticogram using a model trained for spontaneous activity in the rat barrel cortex, Neurosci Res. 87 (2014) 40-48. doi: 10.1016/j.neures.2014.06.010.

31. S.N. Baker, G. Curio, N.L. Roger, EEG oscillations at 600 Hz are macroscopic markers for cortical spike bursts. J Physiol. 550 (2003) 529-534. doi: 10.1113/jphysiol.2003.045674.

32. H. Watanabe, M.A. Sato, T. Suzuki, A. Nambu, Y. Nishimura, M. Kawato, T. Isa, Reconstruction of movement-related intracortical activity from micro-electrocorticogram array signals in monkey primary motor cortex. J. Neural Eng. 9 (2012) 036006. doi: 10.1088/1741-2560/9/3/036006.

33. G. Márton, G. Orbán, M. Kiss, R. Fiáth, A. Pongrácz, I. Ulbert, A Multimodal, SU-8-Platinum-Polyimide Microelectrode Array for Chronic In Vivo Neurophysiology, PloS One 10 (2015) e0145307. http://dx.doi.org/10.1371/journal.pone.0145307.

34. Z. Xiang, S.C. Yen, S. Sheshadri, N. Xue, S.H. Lee, J. Wang, N.V. Thakor, C. Lee, Flexible and self-adaptive neural ribbon with three-dimensional electrodes for sciatic nerve recording. *Conf Proc IEEE Eng Med Biol Soc.* 2015; 3157-3160

35. Z. Xiang, J. Liu, C. Lee, A flexible three-dimensional electrode mesh: An enabling technology for wireless brain–computer interface prostheses, Microsystems & Nanoengineering 2 (2016)

28

16012. doi:10.1038/micronano.2016.12

36. R.A. Green, C.M. Williams, N.H. Lovell, L. A. Poole-Warren, Novel neural interface for implant electrodes: Improving electroactivity of polypyrrole through MWCNT incorporation, J MATER SCI-MATER M 19 (2008) 1625-1629. doi:10.1007/s10856-008-3376-7

37. R. Gerwig, K. Fuchsberger, B. Schroeppel, G. S. Link, G. Heusel, U. Kraushaar, W. Schuhmann, A. Stett, M. Stelzle, PEDOT–CNT composite microelectrodes for recording and electrostimulation applications: fabrication, morphology, and electrical properties, Front. Neuroeng. 5 (2012) 8. doi: 10.3389/fneng.2012.00008

38. E. Castagnola, L. Maiolo, E. Maggiolini, A. Minotti, M. Marrani, F. Maita, A. Pecora, G. N. Angotzi, A. Ansaldo, L. Fadiga, G. Fortunato, D. Ricci, Ultra-flexible and brain-conformable micro-electrocorticography device with low impedance PEDOT-carbon nanotube coated microelectrodes, *Neural Engineering (NER), 2013 6th International IEEE/EMBS Conference on,* San Diego, California, 6 - 8 November 2013; 927-930. doi: 10.1109/NER.2013.6696087

39. S. Chen, W. Pei, Q. Gui, R. Tang, Y. Chen, S. Zhao, H. Wang, H. Chen, PEDOT/MWCNT composite film coated microelectrode arrays for neural interface improvement, Sens. Actuator A-Phys. 193 (2013) 141−148. http://dx.doi.org/10.1016/j.sna.2013.01.033

40. J.K. Chapin. Laminar differences in sizes, shapes and response profiles of cutaneous receptive fields in the rat S1 cortex. Exp. Brain Res. 62 (1986) 549–559. doi: 10.1007/BF00236033

41. D.J. Simons, Response properties of vibrissa units in rat SI somatosensory neocortex, J. Neurophysiol. 41 (1978) 798–820.

42. C.C.H. Petersen, The Functional Organization of the Barrel Cortex, Neuron 56 (2007) 339-355. http://dx.doi.org/10.1016/j.neuron.2007.09.017

43. G.E. Carvell, D.J.Simons, Membrane potential changes in rat SmI cortical neurons evoked by controlled stimulation of mystacial vibrissae, Brain Research 448 (1998) 186-191. http://dx.doi.org/10.1016/0006-8993(88)91118-3

44. J. Winnie, K. Yoshida, and U. G. Hofmann. *In-vivo implant mechanics of flexible, silicon-based*

ACREO microelectrode arrays in rat cerebral cortex. IEEE Transactions on Biomedical Engineering 53(5) (2006): 934-940.

45. Fujifilm. "Durimide® 7500 Photosensitive Polyimide Precoursor." Technical Product Information. Revised May, 2012.

46. M. Jeon, J. Cho, Y. K. Kim, D. Jung, E.-S. Yoon, S. Shin, Il-J. Cho, *Partially flexible MEMS neural probe composed of polyimide and sucrose gel for reducing brain damage during and after implantation*, Journal of Micromechanics and Microengineering 24(2): 025010, 2014

47. T. Stieglitz, H. Beutel, M. Schuettler, J.-U. Meyer, *Micromachined, Polyimide-Based Devices for Flexible Neural Interfaces*, Biomedical Microdevices, 2(4), pp 283–294 (2000)

48. S. Bossi, S. Kammer, T. Doerge, A. Menciassi, K. P. Hoffmann, S. Micera. *Prototype development of an actuated intraneural electrode, IFESS 2008-From Movement to Mind, 13th Annual International FES Society. Conference. Friburgo, Germania, 21 – 25 settembre, 2008*

49. X. Jiang, X. Sui, Y. Lu, Y. Yan, C. Zhou, L. Li, Q. Ren and X. Chai, *In vitro and in vivo evaluation of a photosensitive polyimide thin-film microelectrode array suitable for epiretinal stimulation*, Journal of NeuroEngineering and Rehabilitation 2013, 10:48

50. S. P. Lacour, R. Atta, J.J. FitzGeraldc, M. Blamire, E. Tarte, J. Fawcett, Polyimide micro-channel arrays for peripheral nerve regenerative implants, Sensors and Actuators A: Physical, 147 (2008) 456–463

51. Y. Sun,S. P. Lacour,R. A. Brooks, N. Rushton, J. Fawcett, R. E. Cameron, Assessment of the biocompatibility of photosensitive polyimide for implantable medical device use, J Biomed Mater Res A. 90(3):648-55 2009,

52. G. Paxinos, C. Watson. The Rat Brain in Stereotaxic Coordinates, 6th Edn. Amsterdam: Elsevier (2007)

53. E. Castagnola, A. Ansaldo, E. Maggiolini, G.N. Angotzi, M. Skrap, D. Ricci, L. Fadiga, Biologically compatible neural interface to safely couple nanocoated electrodes to the surface of the brain, ACS Nano 7 (2013) 3887-3895. doi: 10.1021/nn305164c

54. E. Castagnola, E. Maggiolini, L. Ceseracciu, F.Ciarpella, E. Zucchini, S. De Faveri, L. Fadiga, D. Ricci, pHEMA Encapsulated PEDOT-PSS-CNT Microsphere Microelectrodes for Recording Single Unit Activity in the Brain. Front Neurosci.10 (2016) 151. doi:10.3389/fnins.2016.00151

55. N. Mesgarani, C. Cheung, K. Johnson, E. F. Chang, Phonetic Feature Encoding in Human Superior Temporal Gyrus, Science 343 (2014) 1006-1010. DOI: 10.1126/science.1245994

56. E. Castagnola, A. Ansaldo, E. Maggiolini,T. Ius, M. Skrap, D. Ricci, L. Fadiga, Smaller, softer, lower-impedance electrodes for human neuroprosthesis: a pragmatic approach, Front Neuroeng 7 (2014). Doi: 10.3389/fneng.2014.00008.